ISSN 1330-3651 (Print), ISSN 1848-6339 (Online)
Received: 21 April 2025; Accepted: 26 August 2025

https://doi.org/10.17559/TV-20250421002616
Original scientific paper

Analysis of the Effect of Wind Turbines Used In Electric Vehicles on Drag Power

Osama ALMAHMOUD, Abdulhakim KARAKAYA*

Abstract: The increasing role of electric vehicles (EVs) in future transportation systems is of significant importance for improving energy efficiency and environmental sustainability. The integration of renewable energy sources, particularly wind energy, with these vehicles has the potential to reduce energy costs and carbon emissions. This study analyzed how different wind turbine placements influence electric vehicles in terms of drag force. The aerodynamic performance impacts of various configurations were also examined. The drag force on the vehicle was determined based on the turbine location, and the optimal placement was identified. For this purpose, an electric vehicle model was designed, and simulations were conducted using ANSYS (Analysis Systems) software. Additionally, the amount of energy generated was compared with the energy loss caused by the increased drag force. Furthermore, the most efficient integration method for wind turbines in electric vehicles was determined.

Keywords: drag force; electric vehicle; energy; wind turbine

1 INTRODUCTION

The widespread use of gasoline-powered vehicles has led to environmental pollution, increased noise, and a heightened risk of depletion of fossil fuel reserves. Although electric vehicles (EVs) have the potential to address some of these issues, they have not been widely adopted [1, 2]. In EVs, propulsion is provided by electric motors. Batteries that store electrical energy provide the power necessary for motion without burning fossil fuels, producing no emissions. Despite the absence of emissions, the high purchase costs of EVs and their limited range owing to energy storage challenges remain significant concerns. Currently, range limitations continue to hinder the widespread adoption of EVs [3-9]. EVs are charged at fixed stations that draw electricity from grids responsible for supplying residential, commercial, and industrial facilities. This dependence on charging infrastructure may lead to a substantial increase in electricity demand. Research on EV range limitations focuses on two main areas: first, developing batteries with higher specific energy and developing electricity from alternative sources [10, 11]; and second, reducing energy losses in vehicles and reducing a portion of the wasted energy. Renewable energy integration is considered a critical factor in the EV energy supply. However, solar energy systems, which are a renewable source, currently face challenges in vehicular applications owing to their weather dependency, low efficiency, and large space requirements. Thus, integrating environmentally friendly wind turbine systems capable of continuous and efficient operation could enhance their energy efficiency and resolve their range limitations.

Quartey et al. designed a car with a roof-mounted wind turbine to charge batteries using wind energy [12], and the practical results revealed drawbacks, including increased friction forces that reduced the vehicle's efficiency. Lv et al. experimentally investigated the impact of regenerative braking on EV energy efficiency. By analyzing the energy flow with and without regenerative braking, they demonstrated that regenerative braking improved energy efficiency by 11.18% and extended the driving range by 12.58% [13]. Karana and Sahoo found that waste heat recovery via thermoelectric systems increased energy efficiency by 5.78% [14]. Zhang et al. investigated the aerodynamic effects of roof-mounted wind turbines integrated into electric vehicles using Computational Fluid Dynamics (CFD) simulations. They demonstrated that the turbine-induced drag force increased by 8-12%, but noted that a net energy gain remained feasible depending on the wind speed [15]. Patel et al. compared the effects of vertical- and horizontal-axis wind turbines on vehicle aerodynamics and revealed that vertical-axis turbines induce significantly lower drag increments at low speeds [16]. Singh and Gupta reported that optimizing the drag coefficient of multiple small turbines integrated into vehicle bodies reduced energy loss to 4.3% [17]. Rubio and Llopis-Albert published a comprehensive review emphasizing the direct correlation between turbine design, positioning strategies, and aerodynamic efficiency [18]. Existing research highlights the significant limitations of small-scale wind turbines in mobile applications. Jahanfar and Iqbal pointed out their inefficiency, noting that typical urban wind speeds are often too low for net energy gain [19]. The practical energy yield from car-mounted wind turbines remains negligible compared to the power demands of vehicles. Empirical tests by Lee et al. showed that a 0.5 m² turbine at highway speeds (100 km/h) generates only ~40-60 Wh over a 100 km trip, which is less than 0.3% of the energy required to propel an average mid-sized electric vehicle [20]. This is supported by Shahin's 2023 experimental data, which revealed that microturbines on EVs only recover 1.2-3.8% of drag losses in real-world conditions [21]. These studies collectively question the feasibility of wind turbines as standalone range extenders, suggesting the need for hybrid solutions (e.g., solar-wind) or alternative regenerative technologies to offset aerodynamic losses.

However, a systematic comparison of the aerodynamic effects of wind turbines is lacking. This study addresses this gap by analyzing the impact of wind turbine placement on EVs, focusing on aerodynamic drag (C_d) and energy generation through three-dimensional ANSYS Fluent simulations. Two turbine positions (top and front) were tested to quantitatively evaluate the balance between the energy loss (P_{loss}) and gain ($P_{turbine}$). Unlike previous studies, this study specifically examines how turbine position affects the drag coefficient, assesses whether front-mounted turbines can reduce net energy loss, and provides integrated design guidelines for aerodynamic optimization. These findings provide crucial data for

policymakers and engineers involved in renewable energy integration and sustainable mobility.

2 TYPES OF ELECTRIC VEHICLE

Basic electric vehicles (EVs) operate solely via electric propulsion, using batteries as the energy source. Alternatively, they can function in combination with an internal combustion engine (ICE) [22]. Furthermore, alternative energy sources can be used. These vehicles are known as hybrid electric vehicles (HEVs) [23]. Vehicles equipped with both batteries and fuel cells are termed fuel cell electric vehicles (FCEVs) [24, 25]. Based on these distinctions, EVs can be classified into four categories.

2.1 Battery-Electric Vehicle

Battery Electric Vehicles (BEVs) derive their power exclusively from batteries, and the vehicle range depends on the battery capacity [26]. BEVs offer distinct advantages: they have a simple structure, are user-friendly, and are environmentally sustainable [27]. They do not produce greenhouse gases and operate quietly. Electric propulsion enables instant high-torque delivery, even at low speeds [28]. Fig. 1 shows a block diagram of the BEV configuration [26]. In this setup, the batteries supply power to the electric motors through a power converter circuit, and the motors drive the wheels of the vehicle.

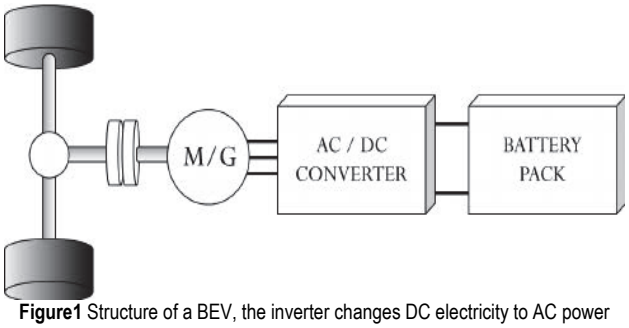

Figure1 Structure of a BEV, the inverter changes DC electricity to AC power [23]

2.2 Hybrid-Electric Vehicle

Hybrid Electric Vehicles (HEVs) are propelled by a combination of an internal combustion engine (ICE) and an electric power transmission (PT) system. This combination can vary in its configuration [29]. HEVs utilize an electric propulsion system under low-power demand conditions [30], providing significant advantages in urban driving scenarios by reducing fuel consumption during engine-idle periods. At higher speed requirements, the vehicle switches to the ICE [31]. These two power systems can also collaborate to enhance their performance. The batteries can be charged either via ICE or through regenerative braking. Thus, HEVs are ICE-powered vehicles supplemented by an electric propulsion system to improve fuel economy [32]. The energy management mechanisms of HEVs are shown in Fig. 2 [33]. Based on the driver inputs, vehicle speed, battery state of charge (SOC), and fuel economy requirements, the system distributes power between the ICE and electric motor.

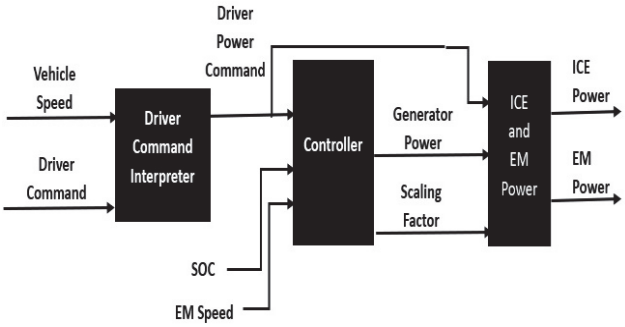

Figure 2 HEV's energy management system

2.3 Plug-in Hybrid-Electric Vehicle

The Plug-in Hybrid Electric Vehicle (PHEV) concept has emerged to extend the all-electric range of Hybrid Electric Vehicles (HEVs) [34, 35]. Similar to HEVs, PHEVs utilize an internal combustion engine (ICE) and an electric power transmission (PT) system; however, in PHEVs, the electric motor serves as the primary drive and requires a larger battery than that of the battery in HEVs. PHEVs operate electrically and engage the ICE only when the battery is depleted [29]. The ICE extends the range of the vehicle by recharging its battery. Unlike HEVs, PHEVs can be charged directly from the grid and can leverage regenerative braking [36]. Because they predominantly operate on electricity, PHEVs exhibit lower carbon footprints [37].

2.4 Fuel-Cell Electric Vehicle

Fuel-cell electric vehicles (FCEVs), also referred to as hydrogen fuel cell vehicles, operate using fuel cells that generate electricity through chemical reactions [38]. FCEVs primarily utilize hydrogen, the most common fuel in this industry, which is stored in specialized, high-pressure tanks. Oxygen, which is required for power generation, is sourced from ambient air. The energy produced by the fuel cells is transferred to an electric motor that drives the vehicle wheels. Excess energy is stored in batteries or supercapacitors [38, 39]. Fig. 3 illustrates the configuration of an FCEV [40].

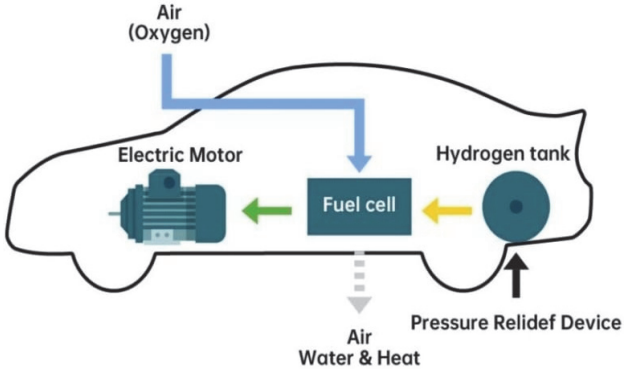

Figure 3 FCEV's configuration [40]

Tab. 1 presents a comparative analysis of the driving components, energy sources, and limitations of the different vehicle types.

Table 1 Comparative analysis of several vehicle types

Type	Driving component	Energy Source	Features	Drawbacks
BEV	EM	Battery, and UC	There are no emissions, the system is not reliant on oil, the range is mostly determined by the battery type, and the system is commercially available [41].	The capacity of the battery, range, recharging time, the accessibility of charging stations, and elevated pricing [42].
HEV	EM and ICE	Battery, UC, and ICE	Low emissions, long range, complicated construction with electrical and mechanical driving trains, and commercially available [43].	Algorithmic complexity in energy distribution and mode transitions. Low energy density limits the contribution of electrical energy. High weight reduces aerodynamic efficiency [43].
FCEV	EM	Fuel cell (FC)	Little emissions, high efficiency, independence from electric power, and commercial availability [44].	The hydrogen distribution infrastructure is extremely limited compared to electric vehicle charging stations. Currently, hydrogen production largely relies on fossil fuels, which undermines its environmental advantages [44].

3 AERODYNAMICSOF VEHICLES

The aerodynamic performance of electric vehicles (EVs) is crucial to their energy efficiency. This study conducted an aerodynamic analysis to examine how the integration of wind turbines influences the airflow behavior around an EV, with a specific focus on changes in the drag force. The drag coefficient (C_d) serves as the primary metric for quantifying aerodynamic efficiency and is derived from ANSYS Fluent simulations using Eq. (1) [45]:

$$C_d = \frac{F_d}{\frac{1}{2}\rho v^2 A} \tag{1}$$

In Eq. (1), C_d is the drag coefficient, where F_d represents the drag force, ρ is the air density, v indicates the wind velocity, and A corresponds to the projected cross-sectional area normal to the flow direction. Vehicle manufacturers aim to attract consumers by designing cars with low drag coefficients [46]. The drag coefficients vary significantly, ranging from approximately 1.0 for large semi-trailers to 0.4 for minivans and 0.3 for passenger cars [46]. Generally, an increase in the bluntness of a vehicle correlates with an increase in its drag coefficient [47]. Findings in this article address discrepancies in existing literature by demonstrating that strategic wind turbine placement can partially offset drag losses. However, complete energy recovery under real-world driving conditions remains unattainable, underscoring the need for further optimization.

4 WIND TURBINE

A wind turbine is a device that converts kinetic energy, known as wind energy, into mechanical energy, a process called wind energy conversion. When mechanical energy is used to generate electricity, the device is referred to as a wind turbine or a wind power plant [48]. Wind turbines are classified into two primary categories as illustrated in Fig. 4: horizontal-axis and vertical-axis. Horizontal-axis machines rotate blades on an axis parallel to the ground, vertical-axis machines rotate blades on an axis perpendicular to the ground. Numerous designs exist for both types, each with unique advantages and disadvantages.

Eq. (2) provides a formula for estimating the wind power extractable from a moving fluid mass [49].

$$P = \frac{1}{2}\rho A v^3 \tag{2}$$

In Eq. (2), P represents wind power, and A is the swept area. Eq. (2) provides all the necessary parameters to estimate the system power output; however, a series of factors must be considered to determine the total efficiency (E) of the system. These include rotor efficiency (E_r), generator efficiency (E_g), and transmission efficiency (E_t) [49]. According to the Betz limit supported by Musgrove, a maximum of 59.3% of wind power can be converted into useful power [50]. A portion of the energy may be lost in the gearbox, bearings, generator, drive train, or other components [51]. Fig. 4 illustrates the different types of wind turbines [52].

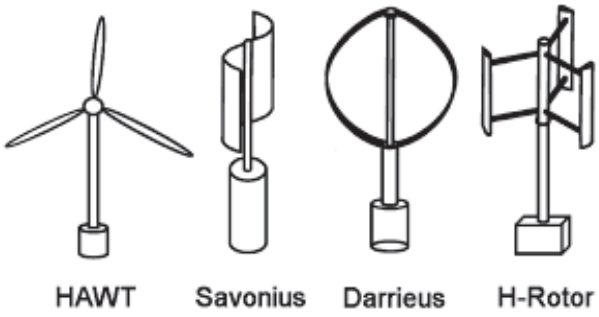

Figure 4 Wind turbine types [49]

5 SIMULATION METHODOLOGY

5.1 Geometric Model

The electric vehicle (Tesla Model S) was modeled three-dimensionally using SolidWorks 2023 software. Complex details, such as small ventilation holes, were simplified, whereas aerodynamic features (streamlined shape, side mirrors, and wheels) were retained. The vehicle dimensions were derived from the official specifications: length L = 4.97 m, width W = 1.97 m, and height H = 1.53 m. The specifications are illustrated in Fig. 5.

Savonius wind turbines are characterized by a simple design consisting of two or more semicircular buckets offset from the rotation axis, forming a scooping cavity to capture wind energy [53]. This design provides a significant advantage: a high starting torque and the ability to operate effectively under low wind speeds and highly

fluctuating wind directions [54]. Owing to their operational characteristics, including robustness, self-starting capability, and effectiveness in variable winds, Savonius turbines are well suited for small-scale distributed power generation applications, such as street lighting, battery charging, and powering remote or off-grid systems [54]. A Savonius-type wind turbine was designed for this study. The turbine comprises three half-cylindrical blades, each 0.8 m long and 0.15 m in diameter. The turbine specifications are shown in Fig. 6.

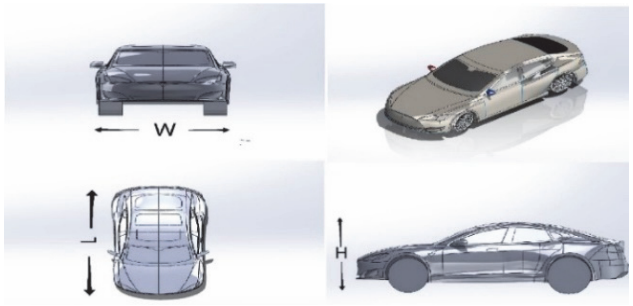

Figure 5 Tesla model S car

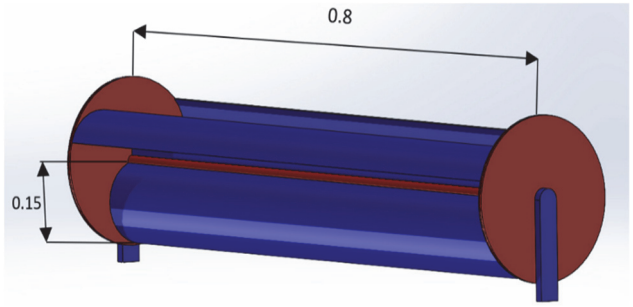

Figure 6 A Savonius type wind turbine

Simulations were conducted for three distinct cases, and the results were compared in terms of drag coefficient (C_d) and net energy (P_{net}). Case A: Vehicle without a turbine. Case B: Turbine mounted on the vehicle's upper surface (turbine center located 2.35 m from the front of the vehicle). Case C: Turbine mounted on the front section of the vehicle (0.48 m above ground level). These three cases are illustrated in Fig. 7.

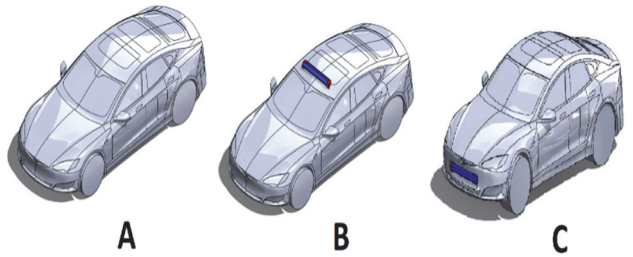

Figure 7 Car and turbine situations

5.2 Domain Boundaries

To ensure simulation accuracy, careful attention was paid to the computational domain boundaries. The domain was defined as follows: 3*L* in front of the vehicle, 6*L* behind it (where *L* is the vehicle length), 2*W* on either side (where *W* is the vehicle width), and 3*H* above it (where *H* is the vehicle height). These boundaries allowed the flow to develop naturally and minimized the boundary effects [55]. The details are shown in Fig. 8 and Fig. 9.

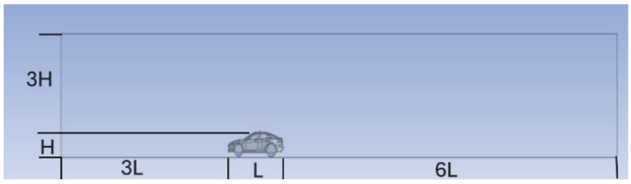

Figure 8 Side view simulation area boundaries

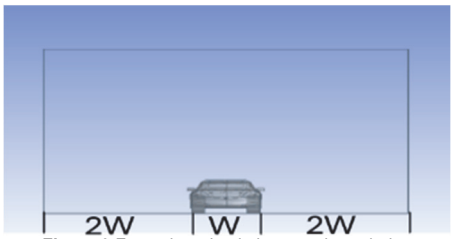

Figure 9 Front view simulation area boundaries

5.3 Meshing

The finite element mesh was optimized for the drag coefficient analysis and consisted of 200,655 nodes and 1,102,511 elements. This configuration ensured precise resolution of the turbine and aerodynamic details while maintaining computational efficiency. Key parameters included: The Base Element Size: A size of 0.8 m with a growth rate of 1.2 to enhance mesh density in critical regions (e.g., turbine and aerodynamic features). Curvature Capture: The "Capture Curvature" algorithm (minimum size: 0.008 m) was used to accurately represent curved surfaces. Computational Optimization: Linear elements and removal of details smaller than 0.004 m reduced the simulation time. The successful transfer of the model to ANSYS Fluent, along with a minimum edge length of $\approx 2.4e^{-5}$ m, validated its efficacy in simulating airflow. The finite element mesh is shown in Fig. 10, and the reference values and boundary conditions are listed in Tab. 2.

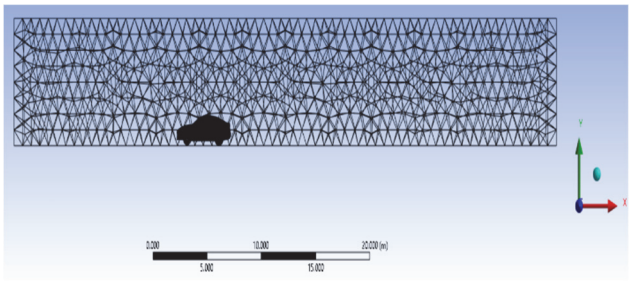

Figure 10 Element mesh

Table 2 Reference values & boundary conditions

Parameter	Value/Setting	Description
Vehicle Mass	1200 kg	Turbine weight is neglected
Density	1.225 kg/m³	Air density under standard conditions
Dynamic Viscosity	1.789×10^{-5} Pa·s	Dynamic viscosity of air used in the simulation
Reference Area	3.321 m²	Area used in calculating aerodynamic forces
Velocity inlet	30 m/s (108 km/h)	The speed of air entering the calculation area.
Pressure Outlet	Atmospheric (1 atm)	Atmospheric pressure condition at the outlet
Flow Type	(Steady-State)	Assumption of time-invariant variables for fast and averaged results
Turbulence Model	*k*-omega SST	Precise model for turbulent flows
Fluid	Air	Fluid used in the simulation

5.4 Mathematical Model of the System

The Navier-Stokes equations are a system of partial differential equations that describe the motion of Newtonian fluids (e.g., water and air). They are used to model flow dynamics in engineering, physics, and applied sciences [56]. Among these, Eq. (4), known as the continuity equation, accounts for the conservation of mass within the fluid. The first term ($\frac{\partial \rho}{\partial t}$) represents the time rate of density change, and the second term $\nabla\cdot(\rho v)$ denotes the mass flow per unit volume. For incompressible fluids (constant density), the equation simplifies to $\nabla\cdot v = 0$:

$$\frac{\partial \rho}{\partial t} + \nabla \cdot (\rho v) = 0 \tag{3}$$

In Eq. (3); ρ: Fluid density (kg/m³), v: Velocity vector (m/s) and t: Time (s).

Eq. (4), the momentum equation (Conservation of Momentum), describes the evolution of the fluid velocity under pressure and viscous forces [56]. The left side includes local and convective accelerations, whereas the right side incorporates the pressure gradient ($-\nabla p$) and viscous forces ($\mu \nabla^2 v$):

$$\rho\left(\frac{\partial v}{\partial t} + v\,.\nabla v\right) = -\nabla p + \mu \nabla^2 v \tag{4}$$

In Eq. (4); ρ Density, v Velocity (m/s), p Pressure (Pa), t Time (s) and μ Dynamic viscosity (Pa.s).

The energy loss (P_{Loss}) and generated energy ($P_{Turbine}$) are derived from Eq. (5) and Eq. (6), respectively, as follows: Tab. 3 and Tab. 4 show the values and results of Eq. (5) and Eq. (6), respectively.

$$P_{loss} = \frac{1}{2}\rho A v^3 C_d \tag{5}$$

Table 3 Values and results of Eq. (5)

Case	ρ / kg/m³	A / m²	v / m/s	C_d	P_{loss} / kW
A	1.225	3.32	30	0.293	16.124
B	1.225	3.56	30	0.33	19.425
C	1.225	3.32	30	0.3	16.787

$$P_{Turbine} = \frac{1}{2}\rho A v^3 C_P \tag{6}$$

Table 4 Values and results of Eq. (6)

Case	ρ / kg/m³	A / m²	v / m/s	C_P	$P_{Turbine}$ / kW
B	1.225	0.24	33	0.4	2.016
C	1.225	0.24	29	0.4	1.575

In Eq. (6); $P_{Turbine}$ wind power, ρ Air density, A Turbine area, C_P Betz coefficient and v Wind speed.

Under practical operating conditions, the inclusion of the turbine mass ($m_{turbine}$) affects the energy consumption during the acceleration and grade-climbing phases. The influence of this added mass was determined using Eq. (7), which accounts for both vehicle acceleration and road grade [57].

$$P_{mass} = m_{turbine} g v \sin\theta + m_{turbine} a v \tag{7}$$

In Eq. (7), $m_{turbine}$ = 20 kg (typical mass for Savonius turbines), g = 9.81 m/s² (gravitational acceleration), v = 30 m/s (constant vehicle speed), θ is the road gradient angle (°), and a is the vehicle acceleration (m/s²). For steady-state conditions (a = 0) and flat roads (θ = 0°), P_{mass} = 0. However, during acceleration ($a \neq 0$) or uphill driving ($\theta \neq$ 0°), this term becomes significant. For example, at θ = 5°, the P_{mass} is equal to 0.513 kW.

6 FINDINGS AND DISCUSSION

6.1 Pressure

In **Case A**, a regular pressure distribution was observed around the vehicle body. High pressure is concentrated at the front owing to the airflow impact on the surface, whereas low pressure is formed at the rear owing to the boundary layer separation and vortex generation. This phenomenon is shown in Fig. 11. The pressure color gradient remained relatively smooth along the body, indicating an aerodynamically optimized design.

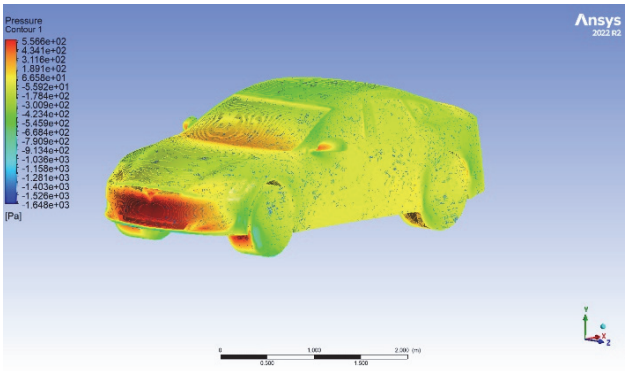

Figure 11 Pressure distribution in case A

In **Case B**, the presence of the top-mounted turbine created a sharp low-pressure zone behind it owing to flow disruption. Additionally, an increase in the high-pressure region on the front wing was observed as the airflow paths were changed. The pressure distribution in this case is illustrated in Fig. 12. Furthermore, the streamlines around the turbine exhibited distortions accompanied by lateral vortices. These changes adversely affect the aerodynamics of vehicles by increasing drag and friction.

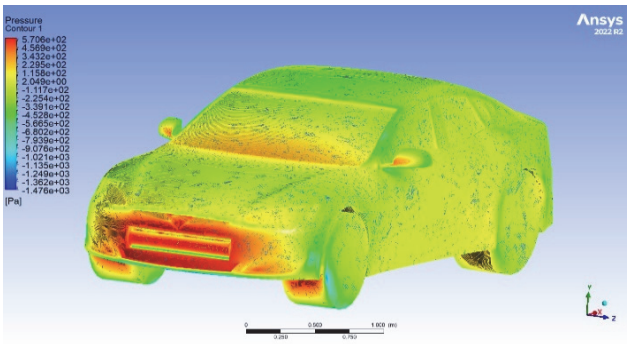

Figure 12 Pressure distribution in case B

In **Case C**, the turbine was positioned at the front of the vehicle, resulting in a high-pressure zone ahead and a

low-pressure zone behind it, which induced vortex formation. A slight improvement in the pressure distribution on the upper surface of the vehicle, compared to Case B, was observed. Fig. 13 illustrates the pressure distribution.

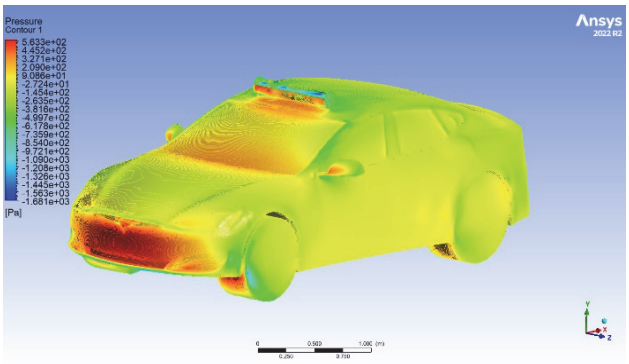

Figure 13 Pressure distribution in case C

In general, it has been determined that the addition of a turbine significantly influences the airflow around the vehicle, leading to alterations in the pressure distribution and the formation of vortices. These changes can adversely affect the aerodynamics of a vehicle by increasing drag and reducing fuel efficiency.

6.2 Velocity Distribution

In **Case A**, the velocity streamlines around the vehicle were regular and parallel, indicating stable aerodynamic flow. High velocities (~46.5 m/s) were observed on the upper surfaces and sides owing to the airflow acceleration over the curved regions. Low-speed zones (< 10 m/s) were concentrated at the rear, resulting from boundary layer separation and vortex formation. The velocity distribution is shown in Fig. 14. Rear vortices account for 60-70% of the total drag, a common characteristic in conventional aerodynamic designs.

In **Case B**, significant turbulence and distortion of the flow streamlines were observed around the turbine. Along the turbine sides, velocity increases of ~40 m/s were detected owing to the narrowing of the airflow path. The velocity distribution in this case is shown in Fig. 15. Compared with Case A, the low-speed zones (< 15 m/s), at the rear of the vehicle expanded, and larger vortices were formed. The turbulence induced by the turbine increased the form drag.

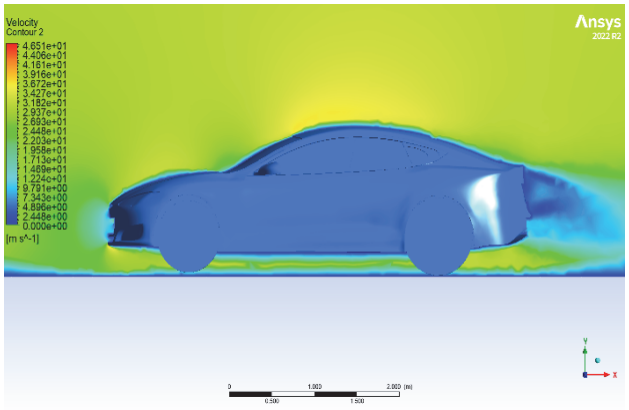

Figure 14 Velocity distribution in case A

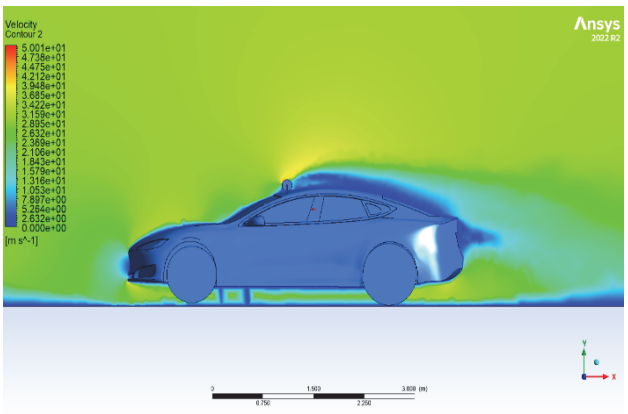

Figure 15 Velocity distribution in case B

In **Case C**, partial airflow redirection around the front turbine was observed, with streamlines being more organized than in Case B. High velocities (~44 m/s) were recorded in front of the turbine, gradually decreasing toward the rear. The rear vortices were smaller than in Case B but remained larger than in Case A. The velocity distribution in this case is illustrated in Fig. 16. Despite the reduced turbulence, the front turbine partially obstructed the forward flow.

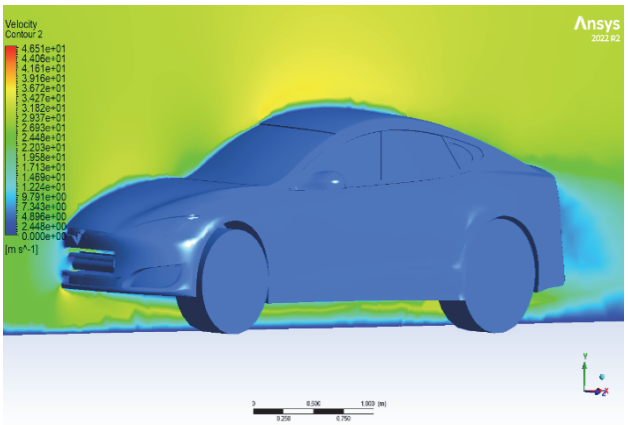

Figure 16 Velocity distribution in case C

6.3 Drag Coefficient Comparison

To assess the aerodynamic implications of turbine placement, drag coefficients (C_d) were extracted for all three cases and are presented with the corresponding error margins derived from the standard deviation of the final 50 iterations post-convergence (Tab. 5). The baseline configuration (Case A) without turbines yielded a drag coefficient of 0.293 ± 0.010, which aligned with the expected aerodynamic efficiency of a sedan-class vehicle [58].

Table 5 Drag coefficients and efficiencies for each case.

Case	C_d	Standard Deviation (±)	Change / %
A	0.293	0.010	-
B	0.33	0.015	12.63%
C	0.3	0.015	2.39%

The inclusion of a top-mounted Savonius turbine (Case B) led to a marked rise in aerodynamic resistance, increasing the drag coefficient to 0.330 ± 0.015, representing a 12.63% increase. This elevation primarily stems from intensified form drag due to flow separation

and enlarged wake vortices generated by the turbine geometry. Additionally, the flow detachment around the turbine body and localized pressure disturbances caused elevated drag loss.

In contrast, positioning the turbine on the front surface of the vehicle (Case C) caused a milder increase in C_d, reaching 0.300 ± 0.015, a 2.39% increase relative to Case A. Although the frontal location still introduced moderate obstruction to the airflow, it yielded a more favorable wake structure with reduced vortex shedding behind the vehicle, improving flow reattachment over the upper surface and partially mitigating pressure drag.

The convergence plots for each simulation (Figs. 17-19) illustrate the residual stabilization behavior. The C_d value fluctuation remained within ±0.1% for 50 iterations. Notably, Case B exhibited slower residual damping, indicating increased turbulence intensity and numerical instability induced by the roof-mounted configuration.

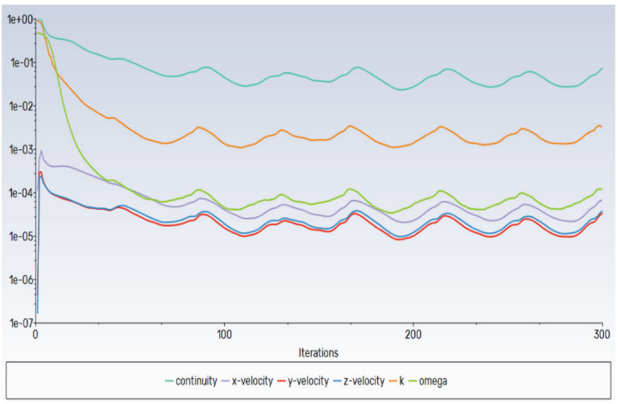

Figure 17 Illustrate the convergence behavior in case A

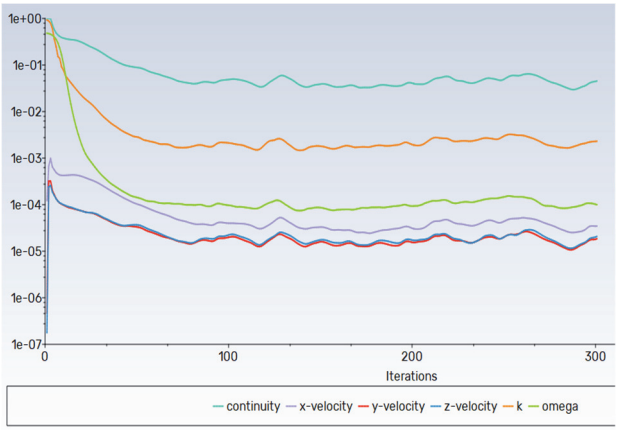

Figure 18 Illustrate the convergence behavior in case B

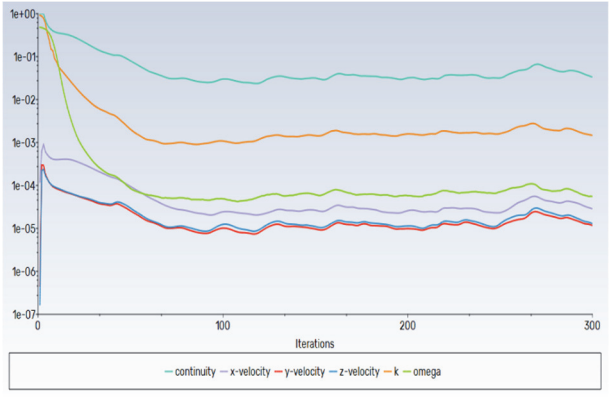

Figure 19 Illustrate the convergence behavior in case C

6.4 Energy Analysis

This study analyzed the impact of wind turbine placement on the energy balance of electric vehicles. As shown in Tab. 6, in the turbine-free case (A), the energy loss due to aerodynamic drag alone was measured at 16.124 kW. The top-mounted turbine (B) increased the energy loss to 19.425 kW (20.5% increase) owing to the higher drag. However, the turbine generated 2.017kW of energy, resulting in a net loss of −17.921kW (calculated using Eq. (8)), which describes the mechanism by which the turbine-generated energy partially offsets the aerodynamic losses. In the front-mounted turbine case (C), the energy loss remained lower, at 16.787 kW (4.1% increase), with 1.576kW of energy generation reducing the net loss to −15.724 kW (2.5% improvement). The results indicate that turbines cannot fully compensate for energy losses in the current design; however, the front-mounted configuration is relatively more efficient. Aerodynamic optimization and hybrid systems are expected to improve this balance.

$$P_{\text{net}} = P_{\text{Turbine}} - P_{\text{loss}} - P_{\text{mass}} \tag{8}$$

Table 6 Energy loss and gained energy values

Case	P_{Loss} / kW	P_{Turbine} / kW	P_{mass} / kW	P_{net} / kW
A	16.124	0.000	0.000	−16.124
B	19.425	2.017	0.513	−17.921
C	16.787	1.576	0.513	−15.724

The results were compared with those of a previous study [59]. Unfortunately, owing to a lack of resources, analyses were performed using the proven ANSYS program instead of a physical experiment for this study. The same study reported a 4.05% drag increase and 5.13% net energy recovery for a turbine embedded in the frontal cavity, consistent with observed 3.95% increase in P_{loss} and 2.5% energy gain (Tab. 6). Minor deviations arise from turbine design differences (Savonius vs. horizontal axis) and vehicle geometry. This convergence validates that frontal integration, when aerodynamically optimized, yields a net positive energy despite the induced drag.

6.5 Analysis of the Range

The battery capacity of the electric vehicle used in this study, based on the Tesla Model S Long Range, was set to 100 kWh. This value was verified through official tests by the U.S. Environmental Protection Agency (EPA) and aligned with the manufacturer's technical specifications [60]. Maintaining a constant battery capacity ensured consistency in the energy loss (P_{net}) and range comparisons. The vehicle range per charge was recalculated based on the turbine positions and a fixed speed of 108 km/h. The range (D) was derived using Eq. (9) [61].

$$D = \frac{E_{\text{bat}}\, v}{P_{\text{net}}} \tag{9}$$

In Eq. (9), E_{bat} = 100 kWh (Tesla Model S Long Range [60]), v = 108 (km/h) and P_{net} Average net energy loss is calculated for each case P_{net}. These calculations assume

P_{net} is independent of speed, a theoretical simplification. In real-world scenarios, P_{net} increases with speed, resulting in lower range values. As shown in Tab. 7, turbine positioning significantly impacted the range.

• **The ideal range** (no turbines) was calculated to be 652 km.

• **The range of Case A (without turbines) increased** by 2.7% to 670 km.

• **The range of Case B (upper-mounted turbine) decreased** by 8.12% to 603 km.

• **Case C** (front-mounted turbine–optimized turbine position) achieved a 5.1% range improvement, reaching 687 km.

These results highlight the critical role of turbine positioning in balancing aerodynamic efficiency and energy consumption.

Table 7 Range values and changes of cases

Case	*D* / km	Change / %
The ideal range	652	-
A	670	+2.7%
B	603	−8.12%
C	687	+5.1%

7 CONCLUSION

This study investigated the aerodynamic and energy trade-offs associated with integrating wind turbines into electric vehicles (EVs), focusing on two configurations: roof-mounted (Case B) and front-mounted (Case C). The results demonstrated that while both configurations increased drag, the front-mounted turbine (Case C) offered a more favorable balance, reducing net energy loss by 2.5% compared to the baseline (Case A) and improving the range by 5.1%. However, the roof-mounted turbine (Case B) significantly increased the drag (12.63%) and reduced the range (8.12%), despite generating slightly more power.

From an economic perspective, the marginal energy gains from wind turbine integration must be critically assessed against system costs, including those of manufacturing, installation, and maintenance. Although front-mounted turbines show promise in partially recovering drag-induced losses, their financial viability remains uncertain, particularly when considering durability challenges and relatively low energy recovery rates (2.5%). Future research should explore hybrid renewable energy systems (e.g., combined solar-wind or regenerative braking) to enhance their cost-effectiveness and reliability.

This study contributes to the field by providing empirical data on the effects of turbine placement, emphasizing the need for aerodynamic optimization in EV design. However, further studies are required to evaluate long-term performance, scalability, and economic feasibility under dynamic driving conditions. Policymakers and engineers should weigh these findings against alternative range-extending technologies to ensure sustainable and economically viable solutions for future mobility.

8 REFERENCES

[1] Xiong, P. & Gu, C. (2017). Starting assistance device for directly-driven electric vehicle with variable-idle speed control. *Technical Gazette/Tehnički Vjesnik*, *24*(1). https://doi.org/10.17559/tv-20151027040734

[2] Siwiec, D., Gawlik, R., & Pacana, A. (2024). Sustainable design of products: Balancing quality, life cycle impact, and social responsibility. *Advances in Production Engineering & Management, 19*(4), 460-488. https://doi.org/10.14743/apem2024.4.519

[3] Liu, Z., Song, J., Kubal, J., Susarla, N., Knehr, K. W., Islam, E., & Ahmed, S. (2021). Comparing total cost of ownership of battery electric vehicles and internal combustion engine vehicles. *Energy Policy*, *158*, 112564. https://doi.org/10.1016/j.enpol.2021.112564

[4] Puma-Benavides, D. S., Izquierdo-Reyes, J., Calderon-Najera, J. D. D., & Ramirez-Mendoza, R. A. (2021). Systematic review of technologies, control methods, and optimization for extended-range electric vehicles. *Applied Sciences*, *11*(15), 7095. https://doi.org/10.3390/app11157095

[5] Kurtulmuş, Z. N. & Karakaya, A. (2024). Efficiency analysis of regenerative brake system using flywheel energy storage technology in electric vehicles. *Tehnicki Vjesnik-Technical Gazette*, *31*(2), 442-448. https://doi.org/10.17559/TV-20230611000719

[6] Kurtulmuş, Z. N. & Karakaya, A. (2023). Review of lithium-ion, fuel cell, sodium-beta, nickel-based, and metal-air battery technologies used in electric vehicles. *International Journal of Energy Applications and Technologies*, *10*(2), 103-113. https://doi.org/10.31593/ijeat.1307361

[7] Kurtulmuş, Z. N. & Karakaya, A. (2024). Review of mechanical, electrochemical, electrical, and hybrid energy storage systems used for electric vehicles. *International Journal of Automotive Science and Technology*, *8*(1), 44-51. https://doi.org/10.30939/ijastech.1357392

[8] Moro, S. R., Cauchick-Miguel, P. A., Sousa-Zomer, T. T. de, & Sousa Mendes, G. H. de. (2023). Design of a sustainable electric vehicle sharing business model in the Brazilian context. *International Journal of Industrial Engineering and Management, 14*(2), 147-161. https://doi.org/10.24867/IJIEM-2023-2-330

[9] Wang, Y. N., Zhang, Z. J., Ping, A., Wang, R. J., & Gong, D. Q. (2024). Optimizing electric vehicle charging strategies using multi-layer perception-based spatio-temporal prediction of charging station load. *Advances in Production Engineering & Management, 19*(4), 443-459. https://doi.org/10.14743/apem2024.4.518

[10] Tran, M. K., Bhatti, A., Vrolyk, R., Wong, D., Panchal, S., Fowler, M., & Fraser, R. (2021). A review of range extenders in battery electric vehicles: Current progress and future perspectives. *World Electric Vehicle Journal*, *12*(2), 54. https://doi.org/10.3390/wevj12020054

[11] Tie, S. F. & Tan, C. W. (2013). A review of energy sources and energy management system in electric vehicles. *Renewable and Sustainable Energy Reviews*, *20*, 82-102. https://doi.org/10.1016/j.rser.2012.11.077

[12] Quartey, G. & Adzimah, S. K. (2014). Generation of electrical power by a wind turbine for charging moving electric cars. *Journal of Energy Technology and Policy*, *4*(3), 1-11.

[13] Lv, C., Zhang, J., Li, Y., & Yuan, Y. (2015). Mechanism analysis and evaluation methodology of regenerative braking contribution to energy efficiency improvement of electrified vehicles. *Energy Conversion and Management*, *92*, 469-482. https://doi.org/10.1016/j.enconman.2014.12.092

[14] Karana, D. R. & Sahoo, R. R. (2021). Experimental study on exergy and sustainability analysis of the thermoelectric based exhaust waste heat recovery system. *International Journal of Exergy*, *34*(1), 1-15.

https://doi.org/10.1504/ijex.2021.112032
[15] Nguefack, M. C. F. et al. (2023). 3D numerical investigation of the air flow in the wake of a compact SUV-type vehicle fitted with optimized horizontal Savonius turbines. *Journal of the Brazilian Society of Mechanical Sciences and Engineering*, *45*(1), 17. https://doi.org/10.1007/s40430-022-03933-w
[16] Patel, U. K., Alom, N., & Saha, U. K. (2025). Lift-based offshore vertical-axis wind turbines for power generation: Current status of technology and future direction of numerical research. *Wind Engineering*, *49*(3), 782-809. https://doi.org/10.1177/0309524X241288094
[17] Singh, P., Gupta, H., Vinayak, O., & Tyagi, A. (2023). Application of response surface method and genetic algorithm in the design of high-efficiency prototype vehicle. *arXiv:2311.04308.* https://doi.org/10.48550/arXiv.2311.04308
[18] Rubio, F. & Llopis-Albert, C. (2021). Analysis of the use of a wind turbine as an energy recovery device in transport systems. *Mathematics*, *9*(18), 2265. https://doi.org/10.3390/math9182265
[19] Jahanfar, A. & Iqbal, M. T. (2021). Design and simulation of a wind turbine powered electric car charging system for St. John's, NL. *2021 IEEE 12th Annual Information Technology, Electronics and Mobile Communication Conference (IEMCON)*, 765-771. https://doi.org/10.1109/IEMCON53756.2021.9623257
[20] Hyman, M. & Ali, M. H. (2022). A novel model for wind turbines on trains. *Energies*, *15*(20), 7629. https://doi.org/10.3390/en15207629
[21] Ebaid, M., Zin Al Abdin, A. E., & Alshawabkeh, M. M. (2023). Numerical analysis and modelling of the effectiveness of micro wind turbines installed in an electric vehicle as a range extender. *SAE International Journal of Electrified Vehicles*, *13*(14-13-02-0010), 191-215. https://doi.org/10.4271/14-13-02-0010
[22] Krithika, V. & Subramani, C. (2018). A comprehensive review on choice of hybrid vehicles and power converters, control strategies for hybrid electric vehicles. *International Journal of Energy Research*, *42*(5). https://doi.org/10.1002/er.3952
[23] Al-Ghaili, A. M., Kasim, H., Aris, H., & Al-Hada, N. M. (2022). Can electric vehicles be an alternative for traditional fossil-fuel cars with the help of renewable energy sources towards energy sustainability achievement. *Energy Informatics*, *5*(Suppl 4), 60. https://doi.org/10.1186/s42162-022-00234-3
[24] Camacho, O. M. F., Nørgård, P. B., Rao, N., & Mihet-Popa, L. (2014). Electrical vehicle batteries testing in a distribution network using sustainable energy. *IEEE Transactions on Smart Grid*, *5*(2), 1033-1042. https://doi.org/10.1109/TSG.2014.2299064
[25] Chan, C. C. (2002). The state of the art of electric and hybrid vehicles. *Proceedings of the IEEE*, *90*(2), 247-275. https://doi.org/10.1109/5.989873
[26] Barreras, J. V., Pinto, C., Schaltz, E., Andreasen, S. J., Rasmussen, P. O., & Araújo, R. E. (2016). Evaluation of a novel BEV concept based on fixed and swappable Li-ion battery packs. *IEEE Transactions on Industry Applications*, *52*(6), 5073-5085. https://doi.org/10.1109/TIA.2016.2585554
[27] Faraz, A., Ambikapathy, A., Thangavel, S., Logavani, K., & Arun Prasad, G. (2021). Battery electric vehicles (BEVs). *Electric Vehicles: Modern Technologies and Trends*, 137-160. https://doi.org/10.1007/978-981-15-9251-5_8
[28] Fernandes, P., Tomás, R., Ferreira, E., Bahmankhah, B., & Coelho, M. C. (2021). Driving aggressiveness in hybrid electric vehicles: Assessing the impact of driving volatility on emission rates. *Applied Energy*, *284*, 116250. https://doi.org/10.1016/j.apenergy.2020.116250
[29] Husain, I. (2021). *Electric and hybrid vehicles: design fundamentals.* CRC Press. https://doi.org/10.1201/9780429490927
[30] Iqbal, M. Y., Wang, T., Li, G., Chen, D., & Al-Nehari, M. M. (2022). A study of advanced efficient hybrid electric vehicles, electric propulsion and energy source. *Journal of Power and Energy Engineering*, *10*(7), 1-12. https://doi.org/10.4236/jpee.2022.107001
[31] Barmaki, R., Ilkhani, M., & Salehpour, S. (2016). Investigation of energy usage and emissions on plug-in and hybrid electric vehicle. *Technical Gazette/Tehnički Vjesnik*, *23*(3). https://doi.org/10.17559/TV-20140928112417
[32] Togun, H., Aljibori, H. S. S., Abed, A. M., Biswas, N., Alshamkhani, M. T., Niyas, H., & Paul, D. (2024). A review on recent advances on improving fuel economy and performance of a fuel cell hybrid electric vehicle. *International Journal of Hydrogen Energy*, *89*, 22-47. https://doi.org/10.1016/j.ijhydene.2024.09.298
[33] Bayindir, K. Ç., Gözüküçük, M. A., & Teke, A. (2011). A comprehensive overview of hybrid electric vehicle: Powertrain configurations, powertrain control techniques and electronic control units. *Energy Conversion and Management*, *52*(2), 1305-1313. https://doi.org/10.1016/j.enconman.2010.09.028
[34] Reddy, K. S. & Veeranna, S. B. (2022). Modified full bridge dual inductive coupling resonant converter for electric vehicle battery charging applications. *International Journal of Power Electronics and Drive Systems*, *13*(2), 773-782. https://doi.org/10.11591/ijpeds.v13.i2.pp773-782
[35] Gao, Y. & Ehsani, M. (2009). Design and control methodology of plug-in hybrid electric vehicles. *IEEE Transactions on Industrial Electronics*, *57*(2), 633-640. https://doi.org/10.1109/TIE.2009.2027918
[36] Veza, I., Asy'ari, M. Z., Idris, M., Epin, V., Fattah, I. R., & Spraggon, M. (2023). Electric vehicles (EV) and driving towards sustainability: Comparison between EV, HEV, PHEV, and ICE vehicles to achieve net zero emissions by 2050 from EV. *Alexandria Engineering Journal*, *82*, 459-467. https://doi.org/10.1016/j.aej.2023.10.020
[37] Xia, X., Li, P., Xia, Z., Wu, R., & Cheng, Y. (2022). Life cycle carbon footprint of electric vehicles in different countries: A review. *Separation and Purification Technology*, *301*, 122063. https://doi.org/10.1016/j.seppur.2022.122063
[38] Miller, J. F., Webster, C. E., Tummillo, A. F., & DeLuca, W. H. (1997). Testing and evaluation of batteries for a fuel cell powered hybrid bus. *Proceedings of the Thirty-Second Intersociety Energy Conversion Engineering Conference (IECEC-97)*, *2*, 894-898. https://doi.org/10.1109/IECEC.1997.661887
[39] Thounthong, P., Raël, S., & Davat, B. (2005). Utilizing fuel cell and supercapacitors for automotive hybrid electrical system. In *Twentieth Annual IEEE Applied Power Electronics Conference and Exposition (APEC 2005)*, 1, 90-96. https://doi.org/10.1109/APEC.2005.1452894
[40] Hasan, F., Ibrahimova, G., & Islam, M. R. (2024). How flexibility helps rapid production of electric vehicles in Azerbaijan. *Global Journal of Flexible Systems Management*, *25*(1), 81-100. https://doi.org/10.1007/s40171-023-00360-1
[41] Grunditz, E. A. & Thiringer, T. (2016). Performance analysis of current BEVs based on a comprehensive review of specifications. *IEEE Transactions on Transportation Electrification*, *2*(3), 270-289. https://doi.org/10.1109/TTE.2016.2571783
[42] Dixon, J. & Bell, K. (2020). Electric vehicles: Battery capacity, charger power, access to charging and the impacts on distribution networks. *eTransportation*, *4*, 100059. https://doi.org/10.1016/j.etran.2020.100059
[43] Sabri, M., Danapalasingam, K. A., & Rahmat, M. F. (2016). A review on hybrid electric vehicles architecture and energy

management strategies. *Renewable and Sustainable Energy Reviews*, *53*, 1433-1442. https://doi.org/10.1016/j.rser.2015.09.036

[44] Chandran, M., Palanisamy, K., Benson, D., & Sundaram, S. (2022). A review on electric and fuel cell vehicle anatomy, technology evolution and policy drivers towards EVs and FCEVs market propagation. *The Chemical Record*, *22*(2), e202100235. https://doi.org/10.1002/tcr.202100235

[45] Roney, J. A. (2023, June). Using free software as computational wind tunnels to teach students about airfoils. *2023 ASEE Annual Conference & Exposition.* https://doi.org/10.18260/1-2--44577

[46] Etukudoh, E. A., Usman, F. O., Ilojianya, V. I., Daudu, C. D., Umoh, A. A., & Ibekwe, K. I. (2024). Mechanical engineering in automotive innovation: A review of electric vehicles and future trends. *International Journal of Science and Research Archive*, *11*(1), 579-589. https://doi.org/10.30574/ijsra.2024.11.1.0081

[47] Hoerner, S. F. (2018). *Fluid-dynamic drag: Practical information on aerodynamic drag and hydrodynamic resistance.* Hoerner Fluid Dynamics. https://doi.org/10.1017/S0001924000034187

[48] Mousavi-Seyedi, S. S., Aminifar, F., Rahimikian, A., & Rezayi, S. (2013). AHP-based prioritization of microgrid generation plans considering resource uncertainties. *2013 Smart Grid Conference (SGC)*, 63-68. https://doi.org/10.1109/SGC.2013.6733800

[49] Abd Kadir, E., Miskon, M. T., Abd Rashid, N., & Yunus, M. Y. (2018). A study of vertical wind turbine for application in low wind speed condition in UiTM Terengganu, Malaysia. *Journal of Power and Energy Engineering*, *6*(08), 38. https://doi.org/10.4236/jpee.2018.68002

[50] Biswas, S. & Chen, J. S. J. (2025). Power coefficient for large wind turbines considering wind gradient along height. *Energies*, *18*(3), 740. https://doi.org/10.3390/en18030740

[51] Li, G. & Zhu, W. (2022). A review on up-to-date gearbox technologies and maintenance of tidal current energy converters. *Energies*, *15*(23), 9236. https://doi.org/10.3390/en15239236

[52] Eriksson, S., Bernhoff, H., & Leijon, M. (2008). Evaluation of different turbine concepts for wind power. *Renewable and Sustainable Energy Reviews*, *12*(5), 1419-1434. https://doi.org/10.1016/j.rser.2006.05.017

[53] Vijayakumar, K., BubeshKumar, D., & Shivakumar, N. (2020). Analysis of magnetic levitated Savonius wind turbine. *IOP Conference Series: Materials Science and Engineering*, *993*(1), 012039. https://doi.org/10.1088/1757-899X/993/1/012039

[54] Homzah, O. F., Widagdo, T., Asrofi, I., & Pratama, D. A. (2021). Prototype of small Savonius wind turbine. *Proceedings of the 4th Forum in Research, Science, and Technology (FIRST-T1-T2-2020).* https://doi.org/10.2991/ahe.k.210205.037

[55] Hamdamov, M., Bozorov, B., Mamataliyeva, H., & Ergashov, D. (2023). Numerical modeling of wind turbine with vertical axis using turbulence model k-ω in ANSYS FLUENT. *E3S Web of Conferences*, 401, 02024. https://doi.org/10.1051/e3sconf/202340102024

[56] Jayawardena, A. W. (2021). *Fluid mechanics, hydraulics, hydrology and water resources for civil engineers.* CRC Press. https://doi.org/10.1201/9780429423116

[57] Ebaid, M. S., Shahin, Z. A. A., & Alshawabkeh, M. M. (2023). Feasibility studies of micro wind turbines installed on electric vehicles as range extenders using real-time analytical simulation with multi driving cycles scenarios. *Advances in Mechanical Engineering*, *15*(4), 16878132231165964. https://doi.org/10.1177/16878132231165964

[58] Yadav, A., Rawal, P., & Mishra, R. K. (2018). Modelling and simulation of aerodynamic performance of vortex generators for hatch back type cars. *Vibroengineering Procedia*, *21*, 131-136. https://doi.org/10.21595/vp.2018.20399

[59] El, E., Yildiz, C., Dandil, B., & Yildiz, A. (2022). Effect of wind turbine designed for electric vehicles on aerodynamics and energy performance of the vehicle. *Thermal Science*, *26.* https://doi.org/10.2298/TSCI2204907E

[60] U. S. Environmental Protection Agency (EPA). (2023). Tesla Model S Long Range: Fuel economy data. Retrieved from https://www.fueleconomy.gov

[61] Zhang, X. & Mi, C. (2011). *Vehicle power management: modeling, control and optimization*. Springer Science & Business Media. https://doi.org/10.1007/978-0-85729-736-5

Contact information:

Osama ALMAHMOUD, MSc
Department of Energy System Engineering,
Faculty of Technology,
Kocaeli 41001, Turkey
E-mail: osamamah95@gmail.com

Abdulhakim KARAKAYA, Assistant Professor
(Corresponding author)
Department of Energy System Engineering,
Faculty of Technology,
Kocaeli 41001, Turkey
E-mail: akarakaya@kocaeli.edu.tr